

# Variational Entropic Optimal Transport

Roman Dyachenko<sup>1</sup> Nikita Gushchin<sup>2,3</sup> Kirill Sokolov<sup>4</sup> Petr Mokrov<sup>2</sup> Evgeny Burnaev<sup>2,3</sup>  
 Alexander Korotin<sup>2,3</sup>

## Abstract

Entropic optimal transport (EOT) in continuous spaces with quadratic cost is a classical tool for solving the domain translation problem. In practice, recent approaches optimize a weak dual EOT objective depending on a single potential, but doing so is computationally not efficient due to the intractable log-partition term. Existing methods typically resolve this obstacle in one of two ways: by significantly restricting the transport family to obtain closed-form normalization (via Gaussian-mixture parameterizations), or by using general neural parameterizations that require simulation-based training procedures. We propose Variational Entropic Optimal Transport (VarEOT), based on an exact variational reformulation of the log-partition  $\log \mathbb{E}[\exp(\cdot)]$  as a tractable minimization over an auxiliary positive normalizer. This yields a differentiable learning objective optimized with stochastic gradients and avoids the necessity of MCMC simulations during the training. We provide theoretical guarantees, including finite-sample generalization bounds and approximation results under universal function approximation. Experiments on synthetic data and unpaired image-to-image translation demonstrate competitive or improved translation quality, while comparisons within the solvers that use the same weak dual EOT objective support the benefit of the proposed optimization principle.

## 1. Introduction

Entropic Optimal Transport (EOT) with quadratic cost is well-established mathematical framework with strong theoretical properties which found a wide application in the generative modeling and especially for unpaired domain

<sup>1</sup>Higher School of Economics, Moscow, Russia <sup>2</sup>Applied AI Institute, Moscow, Russia <sup>3</sup>AXXX, Russia <sup>4</sup>Lomonosov Moscow State University, Moscow, Russia. Correspondence to: Roman Dyachenko <rrdiachenko@edu.hse.ru>, Nikita Gushchin <i.nikita.gushchin@gmail.com>.

Preprint. February 3, 2026.

translation. Despite this, the practical adoption of entropic transport methods has been limited by the lack of efficient and flexible algorithms. Existing approaches typically suffer from at least one of the following drawbacks: they are not simulation-free and rely on costly sampling during training (Mokrov et al., 2024); they require adversarial optimization (Gushchin et al., 2024b); they involve training a sequence of models rather than a single objective (Shi et al., 2023); they impose restrictive parametric forms on the transport plan (Korotin et al., 2024); or they turn out to be too sensitive to the entropic regularization strength (Daniels et al., 2021).

In our paper, we make a decisive step towards solving the drawbacks of existing EOT methods, and propose a novel simulation-free solver based on an innovative variational reformulation of the weak dual EOT objective. We present the following **main contributions**:

1. **Variational dual objective** (§3.1). We derive an equivalent reformulation of the weak dual objective of entropic OT with quadratic cost in which the intractable log-partition term is replaced by an exact variational minimization over an auxiliary positive normalizer.
2. **Simulation-free training solver** (§3.2). Building on this reformulation, we propose a *simulation-free* variational solver that jointly learns the dual potential and the auxiliary normalizer, enabling fully simulation-free training with neural parameterizations (no MCMC).
3. **Learning guarantees** (§3.3). We provide finite-sample learning guarantees for recovery of the entropic OT plan, decomposing error into estimation and approximation terms, and show vanishing approximation error under universal function approximation.
4. **Evaluation** (§5). We evaluate our solver on synthetic data and unpaired image-to-image translation. For the latter, we highlight gains by comparing against other solvers that optimize the same weak dual objective.

## 2. Background

This section provides the necessary background on entropic optimal transport and its optimization using weak dual reformulation. In §2.1, we recall the entropic optimal transport problem with quadratic cost, introduce its weak dual

formulation, and describe the structure of the optimal transport plan induced by the optimal dual potential. In §2.2, we clarify our learning setup. In §2.3, we review existing solvers based on weak dual objective, highlighting two main paradigms: simulation-based optimization via implicit sampling proposed by the authors of EgNOT (Mokrov et al., 2024) and simulation-free methods based on restrictive parametric assumptions proposed by the authors of LightSB (Korotin et al., 2024). This discussion motivates the need for a dual formulation that is both simulation-free and sufficiently expressive, which we address in subsequent §3 by proposing our novel VarEOT solver.

### 2.1. Entropic Optimal Transport with the quadratic cost

Let  $p_0, p_1 \in \mathcal{P}_{ac}(\mathbb{R}^D)$  be the set of absolutely continuous Borel probability measures on  $\mathbb{R}^D$ . Let  $\Pi(p_0, p_1)$  denote the set of couplings (transport plans) on  $\mathbb{R}^D \times \mathbb{R}^D$  with marginals  $p_0$  and  $p_1$ . We write  $\pi(x_0, x_1)$  for a plan density;  $H$  is the differential entropy. The Entropic Optimal Transport (EOT) problem is given by:

$$\text{EOT}_\varepsilon(p_0, p_1) \stackrel{\text{def}}{=} \min_{\pi \in \Pi(p_0, p_1)} \left\{ \underbrace{\mathbb{E}_{\pi(x_0, x_1)} \left[ \frac{\|x_0 - x_1\|^2}{2} \right]}_{\text{optimal transport term}} - \varepsilon \underbrace{\int_{\mathbb{R}^D} H(\pi(\cdot | x_0)) p_0(x_0) dx_0}_{\text{entropic regularization term}} \right\}. \quad (1)$$

The entropic regularization term in (1) is due to (Mokrov et al., 2024). There are equivalent forms of the term (Cuturi, 2013; Léonard, 2014) which differ only by additive constants that do not affect the solution.

The EOT problem admits a unique minimizer  $\pi^*$ , referred to as the EOT plan. While the primal formulation (1) is conceptually appealing, it is computationally inconvenient, since enforcing the marginal constraints  $\pi \in \Pi(p_0, p_1)$  requires optimizing over a complex set of probability measures that does not admit a straightforward parametrization.

**Weak dual form of EOT.** Objective (1) admits the following weak dual representation (Mokrov et al., 2024, Theorem 1):

$$\sup_f \left\{ \underbrace{\mathbb{E}_{p_1(x_1)} f(x_1) - \varepsilon \mathbb{E}_{p_0(x_0)} \log Z(f, x_0)}_{\stackrel{\text{def}}{=} \mathcal{L}(f)} \right\}, \quad (2)$$

the sup is taken over integrable functions  $f : \mathbb{R}^D \rightarrow \mathbb{R}$  and

$$Z(f, x_0) \stackrel{\text{def}}{=} \int_{\mathbb{R}^D} \exp \left( \frac{f(x_1) - \frac{1}{2} \|x_0 - x_1\|^2}{\varepsilon} \right) dx_1 \quad (3)$$

is the partition function.

**Optimal transport plan.** Let  $f^*$  be an optimizer of (2), the corresponding optimal transport plan  $\pi^*$  (Mokrov et al.,

2024, Theorem 1) can be recovered from it. By the disintegration with respect to the source marginal  $p_0$  we have:

$$\pi^*(x_0, x_1) = \pi^*(x_1 | x_0) p_0(x_0), \quad (4)$$

Then the density of conditional distribution  $\pi^*(\cdot | x_0)$  in (4) is directly defined by  $f^*$ :

$$\pi^*(x_1 | x_0) = \frac{1}{Z(f^*, x_0)} \exp \left( \frac{f^*(x_1) - \frac{1}{2} \|x_0 - x_1\|^2}{\varepsilon} \right). \quad (5)$$

### 2.2. Computational EOT setup

In practice, the source and target distributions,  $p_0, p_1$ , as well as the EOT objective (1), could be expressed and treated in different ways. To avoid possible misunderstanding, below we formalize our **practical learning setup**:

We assume that source and target distributions  $p_0$  and  $p_1$  are accessible only by a limited number of i.i.d. empirical samples (datasets)  $\{x_0^1, x_0^2, \dots, x_0^N\} \sim p_0$ ;  $\{x_1^1, x_1^2, \dots, x_1^M\} \sim p_1$ . Our aim is to approximate the optimal conditional plan  $\pi^*(\cdot | x_0)$  (eq. (5)) between entire distributions  $p_0$  and  $p_1$ . The recovered solution should provide the *out-of-sample* estimation, i.e., allow generating samples from  $\pi^*(\cdot | x_0^{\text{new}})$ , where  $x_0^{\text{new}}$  is a new sample from  $p_0$  which is not necessarily present in the train dataset.

This setup falls within **continuous** OT, in contrast to discrete OT (Cuturi, 2013; Peyré et al., 2019), which is designed to compute one-to-one or one-to-many *correspondence* directly between the collections of provided source and target samples. As a result, discrete OT approaches do not naturally accommodate the out-of-sample estimation demanded by continuous OT. In our manuscript, we focus exclusively on continuous OT approaches, treating discrete OT as a considerably different direction.

### 2.3. Existing Weak Dual Formulation Solvers

The practical optimization of problem (2) remains challenging due to the presence of the partition function  $Z(f, x_0)$ , which is, in general, intractable to compute exactly. Below we review two representative strategies to optimize the semi-dual objective: (i) general neural potentials with implicit sampling (EgNOT), and (ii) simulation-free objectives enabled by restrictive parametric transport families (LightSB).

**EgNOT solver.** The authors of EgNOT (Mokrov et al., 2024) solve (2) by parametrizing  $f_\theta$  by a neural network and deriving the gradient of the weak dual objective  $\mathcal{L}(f_\theta)$ :

$$\begin{aligned} \nabla_\theta \mathcal{L}(f_\theta) = & - \mathbb{E}_{p(x_0)} \left[ \mathbb{E}_{\pi_\theta(x_1 | x_0)} [\nabla_\theta f_\theta(x_1)] \right] \\ & + \mathbb{E}_{p_1(x_1)} [\nabla_\theta f_\theta(x_1)], \end{aligned} \quad (6)$$

where  $\pi_\theta(x_1 | x_0)$  is given by:

$$\pi_\theta(x_1|x_0) = \frac{1}{Z(f_\theta, x_0)} \exp\left(\frac{f_\theta(x_1) - \frac{1}{2}\|x_0 - x_1\|^2}{\varepsilon}\right).$$

While flexible, **this approach is not simulation-free**: each evaluation of the loss or its gradient requires sampling from the model distribution  $\pi_\theta(x_1|x_0)$ , which is itself defined implicitly through the neural potential  $f_\theta$ . In practice, this sampling step is carried out using Markov chain Monte Carlo (MCMC) methods (Girolami & Calderhead, 2011; Hoffman et al., 2014; Samsonov et al., 2022), such as Langevin dynamics. However, MCMC-based sampling can be computationally expensive, sensitive to hyperparameters, and slow to mix, especially in high-dimensional settings.

**LightSB solver.** An alternative strategy is proposed in LightSB (Korotin et al., 2024). The authors introduce adjusted potential  $v_\theta$  and parametrization:

$$\pi_\theta(x_1|x_0) = \frac{\exp\left(\langle x_0, x_1 \rangle / \varepsilon\right) v_\theta(x_1)}{c_\theta(x_0)}, \quad (7)$$

where,  $c_\theta(x_0) \stackrel{\text{def}}{=} \int_{\mathbb{R}^D} \exp\left(\langle x_0, x_1 \rangle / \varepsilon\right) v_\theta(x_1) dx_1$  is the normalization. And then consider optimization problem:

$$\min_{v_\theta} \left\{ \mathbb{E}_{p_0(x_0)} \log c_\theta(x_0) - \mathbb{E}_{p_1(x_1)} \log v_\theta(x_1) \right\}. \quad (8)$$

This problem is equivalent to the problem (2) under a different parametrization, specifically:

$$\begin{aligned} v_\theta(x_1) &= \exp\left(-\frac{\|x_1\|^2}{2\varepsilon}\right) \exp\left(\frac{f_\theta(x_1)}{\varepsilon}\right); \\ c_\theta(x_0) &= \exp\left(\frac{\|x_0\|^2}{2\varepsilon}\right) Z(f_\theta, x_0). \end{aligned}$$

To solve the problem in practice, the authors of LightSB circumvent the intractability of normalization  $c_\theta(x_0)$  (equivalent of  $Z(f, x_0)$ , eq. (3)) by directly parameterizing the potential  $v_\theta(x_1)$  in form of a Gaussian mixture:

$$v_\theta(x_1) = \sum_{k=1}^{K'} \alpha_k \mathcal{N}(x_1|r_k, \varepsilon S_k), \quad (9)$$

where  $\theta \stackrel{\text{def}}{=} \{\alpha_k, r_k, S_k\}_{k=1}^{K'}$  are the parameters:  $\alpha_k \geq 0$ ,  $r_k \in \mathbb{R}^D$  and symmetric  $0 \prec S_k \in \mathbb{R}^{D \times D}$ . Such a parameterization restricts conditional density  $\pi(x_1|x_0)$  to form:

$$\pi_\theta(x_1|x_0) = \frac{1}{c_\theta(x_0)} \sum_{k=1}^{K'} \tilde{\alpha}_k(x_0) \mathcal{N}(x_1|r_k(x_0), \varepsilon S_k),$$

where  $\tilde{\alpha}(x_0)$  and  $r_k(x_0)$  are some functions of  $\{\alpha_k, r_k, S_k\}_{k=1}^K$  and  $c_\theta(x_0)$  is given in a closed form:

$$c_\theta(x_0) = \sum_{k=1}^{K'} \tilde{\alpha}_k(x_0).$$

While this parameterization leads to a fully tractable and simulation-free objective, it **restricts the expressiveness of the method**, as it limits admissible transport plans to a rather narrow parametric family.

**Summary.** Existing weak dual solvers trade off between expressiveness and tractability: EgNOT supports flexible potentials but requires MCMC during training, while LightSB is simulation-free but restricts the conditional plan family. Below, we present our novel method, VarEOT, which takes the **best of two worlds** by enabling simulation-free training *without* restricting  $\pi(x_1|x_0)$  to a narrow parametric family.

### 3. Variational Entropic Optimal Transport

In this section, we introduce our variational approach to entropic optimal transport. In §3.1, we derive a new variational dual formulation of the EOT objective that replaces the intractable log-partition function with a tractable variational upper bound, yielding a fully differentiable and simulation-free loss. Building on this formulation, §3.2 presents a practical learning algorithm based on neural parameterization of the dual potential and the auxiliary variational function, together with a Langevin sampling procedure for generating transport samples. We further position our method relative to existing dual solvers and highlight its practical advantages. In §3.3 we conduct the analysis of our method from the perspectives of statistical learning theory (finite sampling learning guarantees and approximation with neural networks). All proofs are situated in Appendix A.

#### 3.1. New Variational Dual Formulation of EOT

Our goal is to propose a weak dual solver that, unlike EgNOT and LightSB, does not require simulation during training and allows for expressive parameterization.

A key challenge in this setting is differentiating through the partition function  $\log Z(f, x_0)$ : as a logarithm of an expectation, it cannot be unbiasedly estimated from finite samples in a straightforward way. To overcome this difficulty, we adopt a variational approximation for the logarithm, which allows us to construct a tractable, differentiable surrogate for the dual objective. The details of this variational approach are formalized in proposition below.

**Proposition 3.1** (Variational bound for the partition function). *The logarithm of partition function  $\log Z(f, x_0)$  admits the variational upper bound:*

$$\begin{aligned} \log Z(f, x_0) &\leq -1 + \xi(x_0) + \frac{D}{2} \log(2\pi\varepsilon) + \\ &\quad \mathbb{E}_{z \sim \mathcal{N}(0, I)} \left[ \exp\left(\frac{f(x_0 + \sqrt{\varepsilon}z)}{\varepsilon} - \xi(x_0)\right) \right], \end{aligned} \quad (10)$$

where  $\xi : \mathbb{R}^D \rightarrow \mathbb{R}$  is an arbitrary integrable function. The upper limit is reached when

$$\xi^*(x_0) = \log Z(f, x_0) - \frac{D}{2} \log(2\pi\varepsilon), \quad (11)$$

i.e., at the (shifted by a constant) log partition function.

Thanks to the obtained estimate, we can obtain tractable simulation-free loss:

**Theorem 3.2** (Variational dual form of EOT). *Let*

$$\begin{aligned} \mathcal{L}(f, \xi) &\stackrel{\text{def}}{=} \varepsilon \left( 1 - \frac{D}{2} \log(2\pi\varepsilon) \right) + \\ &\mathbb{E}_{x_1 \sim p_1} [f(x_1)] - \varepsilon \mathbb{E}_{x_0 \sim p_0} [\xi(x_0)] - \\ &\varepsilon \mathbb{E}_{x_0 \sim p_0} \left[ \mathbb{E}_{z \sim \mathcal{N}(0, I)} \exp \left( \frac{f(x_0 + \sqrt{\varepsilon}z)}{\varepsilon} - \xi(x_0) \right) \right], \end{aligned} \quad (12)$$

Then the entropic optimal transport weak dual formulation admits the following variational form:

$$\text{EOT}_\varepsilon(p_0, p_1) = \sup_f \mathcal{L}(f) = \sup_{f, \xi} \mathcal{L}(f, \xi). \quad (13)$$

The optimal solution  $(f^*, \xi^*)$ , where  $\xi^*$  set by (11), recovers

$$\pi^*(x_1 | x_0) = \frac{(2\pi\varepsilon)^{-\frac{D}{2}}}{\exp(\xi^*(x_0))} \exp \left( \frac{f^*(x_1) - \frac{1}{2}\|x_0 - x_1\|^2}{\varepsilon} \right)$$

This novel variational dual form allow so overcome the original problem of estimation of log partition function  $\log Z(f, x_0)$  in the weak dual form (2).

For convenience we define:

$$\begin{aligned} \pi^{f, \xi}(x_0, x_1) &\stackrel{\text{def}}{=} \frac{(2\pi\varepsilon)^{-\frac{D}{2}} p_0(x_0)}{\exp(\xi(x_0))} \exp \left[ \frac{f(x_1) - \frac{1}{2}\|x_0 - x_1\|^2}{\varepsilon} \right]; \\ \pi^f(x_0, x_1) &\stackrel{\text{def}}{=} \pi^{f, \xi^*}(x_0, x_1), \end{aligned}$$

where  $\xi^*$  is due to (11). The following theorem establishes that the gap between the optimal and current value of the VarEOT objective directly correspond to the KL discrepancy between the recovered measure  $\pi^{f, \xi}$  ( $\pi^f$ ) and EOT plan  $\pi^*$ .

**Theorem 3.3.** *For any measurable functions  $f$  and  $\xi$ ,*

$$\varepsilon \text{KL}(\pi^* \parallel \pi^f) \leq \varepsilon \text{KL}(\pi^* \parallel \pi^{f, \xi}) = \mathcal{L}^* - \mathcal{L}(f, \xi), \quad (14)$$

where  $\text{KL}(\cdot \parallel \cdot)$  denotes the Kullback–Leibler divergence between non-negative measures (see Definition A.1 in Appendix A), and  $\mathcal{L}^*$  is the optimal value of weak dual EOT objective (12).

Our Theorem 3.3 certifies that optimizing objective (12) directly enables us to approximate the ground truth EOT plan. Additionally, eq. (14) suggests that at inference stage it is better to use  $\pi^f$ , not  $\pi^{f, \xi}$ , which we exploit in our practical implementation, see the next section §3.2.

### 3.2. Practical Algorithm

**Training.** The variational formulation derived in Theorem 3.2 leads to a fully tractable and simulation-free optimization objective, given in (12). In practice, we

**Algorithm 1** Training procedure for Variational Entropic Optimal Transport (VarEOT)

---

**Input:** samples from distributions  $p_0$  and  $p_1$ ; entropy regularization parameter  $\varepsilon > 0$ ; batch sizes  $N_0, N_1$ ; number of noise samples  $K$ ; potential network  $f_\theta : \mathbb{R}^D \rightarrow \mathbb{R}$ ; auxiliary network  $\hat{\xi}_\psi : \mathbb{R}^D \rightarrow \mathbb{R}$ .

**Output:** trained potential  $\hat{f}_{\theta^*}$ .

**for** each training iteration **do**

- Sample mini-batches  $\{x_i^0\}_{i=1}^{N_0} \sim p_0$ ,  $\{x_j^1\}_{j=1}^{N_1} \sim p_1$ ;
- Sample i.i.d. noise variables  $z_{i,k} \sim \mathcal{N}(0, I)$  for  $i = 1, \dots, N_0$ ,  $k = 1, \dots, K$ ;
- Compute the empirical loss  $\hat{\mathcal{L}}$  according to eq. (15);
- Update  $\psi, \theta$  by using the gradients  $\nabla_\psi \hat{\mathcal{L}}, \nabla_\theta \hat{\mathcal{L}}$ ;

**end for**

---

parametrize both the potential  $f : \mathbb{R}^D \rightarrow \mathbb{R}$  and the auxiliary variational function  $\xi : \mathbb{R}^D \rightarrow \mathbb{R}$  by neural networks, denoted by  $f_\theta$  and  $\xi_\psi$ , respectively

The resulting training procedure consists of maximizing an empirical estimate of the variational dual loss with respect to both parameter sets  $\theta$  and  $\psi$ . Given mini-batches of samples  $\{x_i^0\}_{i=1}^{N_0} \sim p_0$  from the source distribution and  $\{x_j^1\}_{j=1}^{N_1} \sim p_1$  from the target distribution, the expectations in eq. (12) are approximated using Monte Carlo sampling with i.i.d. Gaussian noise variables  $z_{i,k} \sim \mathcal{N}(0, I)$ , yielding the empirical loss (omitting the additive constant in (12)):

$$\begin{aligned} \hat{\mathcal{L}}(f_\theta, \xi_\psi) &\stackrel{\text{def}}{=} \frac{1}{N_1} \sum_{j=1}^{N_1} f_\theta(x_j^1) - \varepsilon \frac{1}{N_0} \sum_{i=1}^{N_0} \xi_\psi(x_i^0) - \\ &\frac{\varepsilon}{N_0 K} \sum_{i,k=1}^{N_0, K} \exp \left( \frac{f_\theta(x_i^0 + \sqrt{\varepsilon} z_{i,k})}{\varepsilon} - \xi_\psi(x_i^0) \right). \end{aligned} \quad (15)$$

Importantly, **this approximation does not require sampling from the model distribution itself**, in contrast to energy-based approaches such as EgNOT. The complete training procedure is summarized in Algorithm 1.

**Inference.** Following the hint in equation (14), after the training we only use the potential function  $\hat{f}_\theta$  for inference, whereas the function  $\hat{\xi}_\psi$  is not used. The corresponding entropic optimal transport plan is implicitly defined via the conditional distribution (5). To generate samples from this conditional distribution, we employ Langevin dynamics targeting the unnormalized density

$$\pi(x_1 | x_0) \propto \exp \left( \hat{f}_\theta(x_1) - \frac{1}{2\varepsilon} \|x_1 - x_0\|^2 \right).$$

The resulting sampling procedure is detailed in Algorithm 2. In all experiments, we observe that  $10^1$ – $10^3$  Langevin steps with proper step size is enough to get high-quality samples.

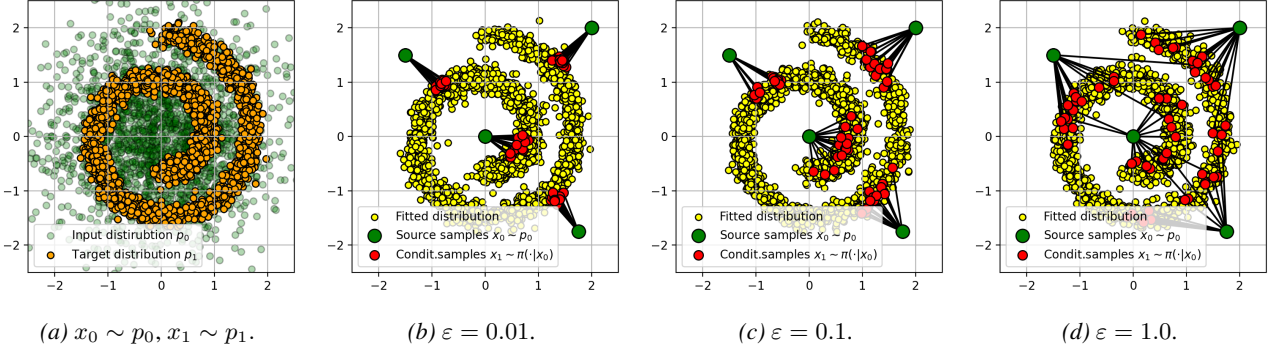


Figure 1. Optimal plan learned with VarEOT (ours) in Gaussian → Swiss roll example.

**Algorithm 2** Langevin sampling from the VarEOT conditional distribution

**Input:** source sample  $x_0 \sim p_0$ ;  
 trained potential network  $\hat{f}_\theta$ ;  
 entropy regularization  $\varepsilon > 0$ ;  
 number of Langevin steps  $S$ ; step size  $\eta > 0$ .  
**Output:** sample  $x_1 \sim \pi(\cdot | x_0)$ .  
 Initialize  $x_1^{(0)} = x_0$ ;  
**for**  $s = 1$  **to**  $S$  **do**  
 Sample  $z^{(s)} \sim \mathcal{N}(0, I)$ ;  
 $h = \left( \nabla_{x_1} \hat{f}_\theta(x_1^{(s-1)}) - \frac{1}{\varepsilon} (x_1^{(s-1)} - x_0) \right)$ ;  
 Update:  

$$x_1^{(s)} \leftarrow x_1^{(s-1)} + \eta h + \sqrt{2\eta} z^{(s)};$$
  
**end for**  
**Return**  $x_1^{(S)}$

To highlight the practical advantages of VarEOT, we compare it with two representative dual-solver approaches: EgNOT (Mokrov et al., 2024) and LightSB (Korotin et al., 2024) (cf. §2.3). Table 1 summarizes their properties in terms of simulation-free training and structural constraints on the transport plan.

*Table 1.* Comparison of dual solvers for entropic OT.  
 “Simulation-free” indicates whether the method avoids sampling from the model during training. “Not Restricted parameterization” indicates whether the conditional plan is not restricted to a predefined family (e.g., Gaussian mixtures).

Method	Simulation-free training	Not restricted parameterization
EgNOT	✗	✓
LightSB	✓	✗
VarEOT (ours)	✓	✓

VarEOT combines the best of both worlds: it is *simulation-free*, unlike EgNOT, and it does not impose a *restricted parameterization* on the conditional plan, unlike LightSB.

### 3.3. Finite Sample Learning Guarantees

In this subsection we quantify the discrepancy between the transport plan recovered by VarEOT and the ground truth EOT solution. Our method does not have access to  $(p_0, p_1)$  explicitly; instead it works with finite samples (see our computational setup §2.2) and with potentials restricted to parametric classes. This naturally introduces several sources of error in practice: *finite-sample error* (we only observe i.i.d. datasets of sizes  $N$  and  $M$  from  $p_0$  and  $p_1$ ); *function class restriction* (we optimize over class of neural networks rather than over all continuous potentials); *optimization error* (stochastic training, finite-time optimization). Our rigorous theoretical analysis below focuses on the first two items. The third item depends on the chosen optimizer and sampling scheme and is treated separately in practice.

In the results stated below, the function classes  $\mathcal{F}$  and  $\Xi$  should be understood as elements of an increasing sequence of neural-network classes. Specifically, fix an activation function  $\sigma : \mathbb{R} \rightarrow \mathbb{R}$  that is continuous and non-polynomial (e.g., ReLU, GELU, or tanh). For each  $n \geq 1$ , let

$$\mathcal{F}_n := \text{NN}_n^\sigma(D, 1), \quad \Xi_n := \text{NN}_n^\sigma(D, 1), \quad (16)$$

denote neural-network classes of increasing capacity (e.g., in width or number of hidden units). When bounding the estimation error, the specific index  $n$  is not essential for the statement, and we therefore often suppress it and write  $\mathcal{F}$  and  $\Xi$  for simplicity.

In the following theorem we establish the decomposition of the KL discrepancy between ground truth EOT optimal plan  $\pi^*$  and the learned plan  $\pi^{\hat{f}}$  (recall eq. (14)), where

$$\hat{f} = \arg \max_{f \in \mathcal{F}} \widehat{\mathcal{L}} \left( f, Z(f, \cdot) - \underbrace{\frac{D}{2} \log(2\pi\varepsilon)}_{=\xi^*} \right).$$

In particular, we restrict attention to the plan  $\pi^{\hat{f}}$ , since this is the plan used at inference time, see §3.2.

**Proposition 3.4.** *The following bound holds:*

$$\begin{aligned} \varepsilon \mathbb{E} \left[ \text{KL}(\pi^* \parallel \pi^{\hat{f}}) \right] &\leq 2 \underbrace{\mathbb{E} \sup_{f \in \mathcal{F}, \xi \in \Xi} \left| \mathcal{L}(f, \xi) - \hat{\mathcal{L}}(f, \xi) \right|}_{\text{Estimation error}} + \\ &\quad \underbrace{\mathcal{L}^* - \sup_{f \in \mathcal{F}, \xi \in \Xi} \mathcal{L}(f, \xi)}_{\text{Approximation error}}, \end{aligned} \quad (17)$$

where the expectations are taken w.r.t. the random realization of the datasets.

The next theorem states that if we restrict potentials to  $M$ -bounded and  $L$ -Lipschitz families  $\text{Lip}_{L, M}$  and assume compact supports  $X_0 := \text{supp}(p_0)$  and  $X_1 := \text{supp}(p_1)$ , then the estimation error in Proposition 3.4 sublinearly decays to zero as the dataset sizes increase.

**Theorem 3.5** (Bound on estimation error). *Assume that  $\mathcal{F} \subset \text{Lip}_{L_f, M_f}(X_1)$  and  $\Xi \subset \text{Lip}_{L_\xi, M_\xi}(X_0)$ . Then*

$$\begin{aligned} \mathbb{E} \sup_{f \in \mathcal{F}, \xi \in \Xi} \left| \mathcal{L}(f, \xi) - \hat{\mathcal{L}}(f, \xi) \right| &\leq \\ &\leq O\left(N^{-\frac{1}{1+D}}\right) + O\left(M^{-\frac{1}{1+D}}\right) \end{aligned} \quad (18)$$

where hidden constants depend on  $D, L_f, L_\xi, M_f, M_\xi$  and diameters of  $X_0$  and  $X_1$ .

*Remark 3.6.* We note that assuming Lipschitz regularity of the dual potentials is well motivated both theoretically and practically. First, since the supports  $X_0$  and  $X_1$  are compact, it is natural to restrict attention to potentials that are Lipschitz on these sets; moreover, any Lipschitz function defined on a subset of a metric space admits a Lipschitz extension to the ambient space, and one may additionally enforce boundedness by clipping, which preserves Lipschitz constants. Second, neural networks with Lipschitz activation functions are Lipschitz provided the weight operator norms are controlled; in practice, this can be achieved via norm constraints such as spectral normalization.

We now show that the Approximation error in Proposition 3.4 can be made arbitrarily small by choosing sufficiently expressive neural-network classes.

**Theorem 3.7** (Vanishing of approximation error). *Let the sequences of classes  $\{\mathcal{F}_n\}_{n \geq 1}$  and  $\{\Xi_n\}_{n \geq 1}$  be defined as in (16). Then for any  $\delta > 0$  there exists  $n \in \mathbb{N}$  such that*

$$\mathcal{L}^* - \sup_{f \in \mathcal{F}_n, \xi \in \Xi_n} \mathcal{L}(f, \xi) < \delta. \quad (19)$$

**Summary.** Combining these results yields the standard learnability picture for EOT plan recovery: with enough data (large  $N, M$ ) the estimation/generalization gap becomes small, and with sufficiently expressive neural networks the approximation error becomes small.

**Relation to prior work.** Related error decompositions appear in (Mokrov et al., 2024; Kolesov et al., 2024). While (Mokrov et al., 2024) does not provide a fully detailed breakdown of the individual error terms for EgNOT, (Kolesov et al., 2024) develops a finer-grained statistical analysis but for a different objective (entropic barycenters). We follow a similar template, yet provide a detailed analysis for our more elaborate variationally derived VarEOT functional.

## 4. Related Work

In this section, we review the existing continuous EOT approaches, and briefly compare them with our solver. For clarity, we introduce a taxonomy of the existing approaches below, based on the utilized mathematical framework.

**Weak dual EOT** (a.k.a. *semi*-dual EOT) methods (Mokrov et al., 2024; Korotin et al., 2024) optimize the objective eq. (2). They are the most similar to our VarEOT in terms of methodology. The detailed discussion of the approaches is given in §2.3. Crucially, our proposed method successfully overcomes the limitations of existing weak dual approaches while retaining their advantages.

**Dual EOT** (Genevay et al., 2016; Seguy et al., 2018; Daniels et al., 2021) take the advantage of an alternative dual form of the EOT. These methods simultaneously optimize a *pair* of dual potentials  $(u, v)$  in a max max optimization procedure known as Sinkhorn algorithm. While bearing certain resemblance to our VarEOT (e.g., simulation-free training), dual EOT approaches have a number of pitfalls underscoring their performance:

- Dual potentials  $(u, v)$  do not fully recover the (conditional) EOT  $\pi^*(\cdot | x_0)$ . In particular, an *auxiliary* score-based model for the target distribution  $p_1$  is required to enable sampling from  $\pi^*(\cdot | x_0)$  (Daniels et al., 2021). Otherwise, there are only some heuristics (e.g., barycentric projection) that allow the recovered solution to be cast as a *generative* model capable of data-to-data translation (Genevay et al., 2016; Seguy et al., 2018).
- Due to optimization peculiarities, dual EOT approaches turn to be unstable under small regularization coefficient  $\varepsilon$ . This behavior is reported in (Daniels et al., 2021, §5.1) and supported by (Mokrov et al., 2024, §4.2, §C.2).

Overall, our proposed VarEOT seems to provide more user-friendly and production-ready framework with less engineering overhead required to adapt the method to applications.

**Schrödinger bridge (SB)** methods (De Bortoli et al., 2021; Vargas et al., 2021; Chen et al., 2022; Gushchin et al., 2023; Shi et al., 2023; Tong et al., 2024; Gushchin et al., 2024b; De Bortoli et al., 2024; Gushchin et al., 2024a) cast the EOT in a dynamic manner and recover a solution in a form of stochastic differential equation with learnable drift, with the endpoints given by source  $p_0$  and target  $p_1$  distributions. The underlining principles of SB-based approaches are differ-



Figure 2. Qualitative comparison for *Man → Woman* translation with  $\varepsilon = 1.0$ . From top to bottom: input samples, VarEOT (ours), LightSB, and EgNOT. Input images are selected from the test set: we take the first 300 samples and rank them by encoder-decoder reconstruction quality (LPIPS), displaying the top-ranked examples.

ent, e.g., adversarial optimization, gradual iterative markovian/proportional fitting procedure. However, compared to our method, **majority** of them are not simulation-free at training. The exceptions are (Tong et al., 2024) (based on mini-batch EOT approximation, which may be not accurate) and (Gushchin et al., 2024a) (similar to (Korotin et al., 2024) uses restricted Gaussian mixture approximation).

## 5. Experimental Illustrations

We evaluate VarEOT on both synthetic and real-world data. Section 5.1 presents illustrative two-dimensional experiments demonstrating the effect of the regularization parameter  $\varepsilon$  on the learned transport plan. Section 5.2 provides a comprehensive evaluation on unpaired image-to-image translation using the standard ALAE latent space protocol, comparing VarEOT against related entropic transport baselines across multiple translation tasks and regularization regimes. Technical details, including architecture specifications and hyperparameters, are provided in Appendix B.

### 5.1. Two-dimensional Examples

We begin with a standard illustrative two-dimensional experiment that provides intuition into the role of the entropy regularization parameter  $\varepsilon$  in shaping the learned conditional transport plan  $\pi_\theta(x_1 | x_0)$ . Specifically, we consider a setting in which a Gaussian source distribution is transported to a Swiss Roll target distribution. We apply our method for

$\varepsilon \in \{10^{-2}, 10^{-1}, 10^0\}$ , and visualize the resulting transport maps in Fig. 1.

For small values of  $\varepsilon$ , the learned transport is nearly deterministic, with little variation in sampling endpoints. As  $\varepsilon$  increases, the transport becomes progressively more stochastic: the end point diversify, and the conditional distributions  $\pi_\theta(x_1 | x_0)$  spread over a wider region of the target space.

### 5.2. Unpaired Image-to-Image Translation

Unpaired image-to-image translation is a standard benchmark in the entropic optimal transport (EOT) and Schrödinger Bridge (SB) literature (Zhu et al., 2017; Daniels et al., 2021; Chen et al., 2021), as it naturally combines high-dimensional data and the need for stochastic transport plans. In particular, translation in the latent space of pretrained autoencoders has become a popular and convenient setup for comparing entropic transport methods

We follow the widely adopted ALAE protocol (Korotin et al., 2024; Theodoropoulos et al., 2024; Gushchin et al., 2024a; Kornilov et al., 2024; Gazdieva et al., 2024; Han et al., 2025) based on ALAE autoencoder (Pidhorskyi et al., 2020). Specifically, we use a pretrained ALAE autoencoder trained on the full  $1024 \times 1024$  FFHQ dataset (Karras et al., 2019), which contains approximately 70K human face images. The first 60K images are used for training and are split into (*male, female*) and (*child, adult*) subsets. Using the fixed

$\varepsilon$	Task	FID $\downarrow$						LPIPS $\downarrow$					
		LightSB		EgNOT		VarEOT (ours)		LightSB		EgNOT		VarEOT (ours)	
		NFE=10	NFE=1000	NFE=2	NFE=10	NFE=1000	NFE=10	NFE=10	NFE=1000	NFE=2	NFE=10	NFE=1000	
0.1	M $\rightarrow$ F	8.77	13.4	<b>7.63</b>	181.44	11.70	12.74	0.582	0.6	0.585	0.872	0.580	<b>0.570</b>
	F $\rightarrow$ M	10.87	14.9	<b>6.33</b>	248.76	17.00	13.98	0.597	0.603	0.598	0.833	0.586	<b>0.578</b>
	A $\rightarrow$ C	15.42	40.28	<b>10.52</b>	247.81	50.35	17.33	0.577	0.586	0.588	0.839	<b>0.545</b>	0.577
	C $\rightarrow$ A	13.46	18.47	<b>10.4</b>	253.59	21.48	20.13	0.594	0.602	0.608	0.865	0.591	<b>0.590</b>
0.5	M $\rightarrow$ F	19.09	35.4	14.07	<b>9.04</b>	9.50	9.77	0.611	0.718	0.594	0.619	0.600	<b>0.598</b>
	F $\rightarrow$ M	25.81	51.73	11.66	20.01	<b>10.02</b>	<b>9.94</b>	0.628	0.695	0.613	<b>0.609</b>	0.619	0.616
	A $\rightarrow$ Y	22.30	74.25	<b>18</b>	78.85	26.38	25.99	0.608	0.702	0.603	<b>0.593</b>	0.617	0.613
	C $\rightarrow$ A	22.70	40.38	16.95	17.83	<b>16.55</b>	16.74	<b>0.614</b>	0.7	0.629	0.632	0.616	<b>0.614</b>
1.0	M $\rightarrow$ F	22.63	39.41	17.58	10.38	<b>9.59</b>	9.71	0.637	0.749	0.634	0.633	0.613	<b>0.610</b>
	F $\rightarrow$ M	20.97	66.64	26.21	15.21	10.52	<b>10.28</b>	0.649	0.72	0.634	0.654	0.633	<b>0.630</b>
	A $\rightarrow$ C	24.43	60.57	28.45	53.39	<b>16.60</b>	16.83	0.634	0.724	0.623	0.700	0.610	<b>0.608</b>
	C $\rightarrow$ A	24.87	51.48	23.68	<b>15.73</b>	16.55	16.70	0.637	0.733	0.661	0.638	0.623	<b>0.619</b>
10.0	M $\rightarrow$ F	31.85	37.61	26.68	<b>21.84</b>	21.97	22.38	0.680	0.755	0.735	0.625	0.621	<b>0.620</b>
	F $\rightarrow$ M	34.47	63.73	36	<b>25.55</b>	28.84	29.24	0.693	0.758	0.734	0.637	0.632	<b>0.630</b>
	A $\rightarrow$ C	<b>31.85</b>	92.6	64.85	49.84	50.72	51.20	0.680	0.767	0.763	0.619	<b>0.615</b>	<b>0.615</b>
	C $\rightarrow$ A	35.35	51.74	35.53	<b>31.01</b>	32.84	34.07	0.683	0.748	0.741	0.639	0.636	<b>0.633</b>

Table 2. Comparison of unpaired I2I translation methods in the ALAE latent space. We report FID and LPIPS (lower is better) for four translation tasks (M  $\rightarrow$  F, F  $\rightarrow$  M, A  $\rightarrow$  C, C  $\rightarrow$  A) across different values of the entropic regularization  $\varepsilon$ . VarEOT results are shown for different numbers of Langevin inference steps (NFE = 2, 10, 10<sup>3</sup>). For each row, the best-performing method is highlighted in **bold**.

ALAE encoder, we extract 512-dimensional latent representations  $\{z_0^n = \text{Enc}(x_0^n)\}_{n=1}^N$  and  $\{z_1^m = \text{Enc}(x_1^m)\}_{m=1}^M$  corresponding to the source and target domains. We consider 4 setups: male to female (M  $\rightarrow$  F), female to male (F  $\rightarrow$  M), adult to child (A  $\rightarrow$  C), and child to adult (C  $\rightarrow$  A).

**Training.** Given unpaired samples from the two latent distributions, we learn a latent entropic optimal transport plan  $\pi_\theta(z_1 | z_0)$  using our variational formulation. The model is trained entirely in latent space and does not require paired data or image-level supervision.

**Inference.** To translate a previously unseen image  $x_0^{\text{new}}$  (from the remaining 10K test images), we (i) encode it as  $z_0^{\text{new}} = \text{Enc}(x_0^{\text{new}})$ , (ii) sample  $z_1 \sim \pi_\theta(z_1 | z_0^{\text{new}})$  using Langevin dynamics, and (iii) decode  $x_1 = \text{Dec}(z_1)$ .

**Evaluation Protocol.** We evaluate the quality of generated samples using two metrics: Fréchet Inception Distance (FID) (Heusel et al., 2017) and Learned Perceptual Image Patch Similarity (LPIPS) (Zhang et al., 2018). FID is computed between the set of test translated images  $\{x_1^n = \text{Dec}(z_1^n)\}_{n=1}^N$ , where  $z_1^n \sim \pi_\theta(z_1 | z_0^n)$ , and the set of ALAE-reconstructed target images  $\{\tilde{x}_1^m = \text{Dec}(\text{Enc}(x_1^m))\}_{m=1}^M$ . LPIPS is measured between the source  $x_0$  and the translated  $x_1 = \text{Dec}(z_1)$ , where  $z_1 \sim \pi_\theta(z_1 | \text{Enc}(x_0))$ . It measures the input-output similarity.

**Results.** We comprehensively evaluate VarEOT across all four translation setups: M  $\rightarrow$  F, F  $\rightarrow$  M, A  $\rightarrow$  C, and C  $\rightarrow$  A. Figure 2 shows qualitative results for the M  $\rightarrow$  F setup with  $\varepsilon = 1.0$ . We report translations obtained using different numbers of Langevin steps at inference time (NFE = 2, 10, 1000), demonstrating that VarEOT produces visually plausible and stable results even with a very small number of sampling steps. Additional results for alternative translation directions (F  $\rightarrow$  M, A  $\rightarrow$  C, C  $\rightarrow$  A) are pro-

vided in Appendix C (Figures 3, 4, and 5), confirming consistent behavior across all setups. Quantitative evaluation using FID and LPIPS metrics is summarized in Table 2, covering a wide range of regularization parameters  $\varepsilon \in \{0.1, 0.5, 1.0, 10.0\}$  and all four translation directions. We compare VarEOT against closely related entropic transport baselines: LightSB and EgNOT, showing competitive or improved performance across all considered regimes.

A qualitative analysis of the effect of the regularization parameter  $\varepsilon$  on sample diversity provided in Figure 6, illustrating how varying  $\varepsilon$  controls the trade-off between transport cost and output stochasticity. Finally, Figure 7 provides an in-depth study of FID performance as a function of the Langevin step size and the number of inference steps.

## 6. Discussion

**Potential impact.** By introducing an exact variational reformulation of the weak dual EOT objective, VarEOT makes a step toward more efficient entropic transport algorithms that avoid the key limitations of existing methods, such as simulation-based training, adversarial objectives, and restrictive parametric assumptions.

**Limitations.** While VarEOT enables simulation-free training, sampling at inference time via Langevin dynamics is still required, making generation quality dependent on step size and the number of steps. Additionally, the exponential terms in the objective may cause numerical instability if not handled carefully.

## Impact Statement

This paper presents work whose goal is to advance the field of Machine Learning. There are many potential societal consequences of our work, none of which we feel must be specifically highlighted here.

## References

Chen, T., Liu, G.-H., and Theodorou, E. Likelihood training of schrödinger bridge using forward-backward SDEs theory. In *International Conference on Learning Representations*, 2022. URL <https://openreview.net/forum?id=nioAdKCEdXB>.

Chen, Y., Georgiou, T. T., and Pavon, M. Stochastic control liaisons: Richard sinkhorn meets gaspard monge on a schrodinger bridge. *SIAM Review*, 63(2):249–313, 2021.

Cuturi, M. Sinkhorn distances: Lightspeed computation of optimal transport. *Advances in neural information processing systems*, 26, 2013.

Daniels, M., Maunu, T., and Hand, P. Score-based generative neural networks for large-scale optimal transport. *Advances in neural information processing systems*, 34: 12955–12965, 2021.

De Bortoli, V., Thornton, J., Heng, J., and Doucet, A. Diffusion schrödinger bridge with applications to score-based generative modeling. *Advances in neural information processing systems*, 34:17695–17709, 2021.

De Bortoli, V., Korshunova, I., Mnih, A., and Doucet, A. Schrodinger bridge flow for unpaired data translation. *Advances in Neural Information Processing Systems*, 37: 103384–103441, 2024.

Gazdieve, M., Asadulaev, A., Burnaev, E., and Korotin, A. Light unbalanced optimal transport. *Advances in Neural Information Processing Systems*, 37:93907–93938, 2024.

Genevay, A., Cuturi, M., Peyré, G., and Bach, F. Stochastic optimization for large-scale optimal transport. *Advances in neural information processing systems*, 29, 2016.

Girolami, M. and Calderhead, B. Riemann manifold langevin and hamiltonian monte carlo methods. *Journal of the Royal Statistical Society: Series B (Statistical Methodology)*, 73(2):123–214, 2011.

Gottlieb, L.-A., Kontorovich, A., and Krauthgamer, R. Adaptive metric dimensionality reduction. *Theoretical Computer Science*, 620:105–118, 2016. doi: 10.1016/j.tcs.2015.10.040. Full version available as arXiv:1302.2752.

Gushchin, N., Kolesov, A., Korotin, A., Vetrov, D. P., and Burnaev, E. Entropic neural optimal transport via diffusion processes. *Advances in Neural Information Processing Systems*, 36:75517–75544, 2023.

Gushchin, N., Kholkin, S., Burnaev, E., and Korotin, A. Light and optimal schrödinger bridge matching. In *Forty-first International Conference on Machine Learning*, 2024a.

Gushchin, N., Selikhanovych, D., Kholkin, S., Burnaev, E., and Korotin, A. Adversarial schrödinger bridge matching. *Advances in Neural Information Processing Systems*, 37: 89612–89651, 2024b.

Han, D.-S., Kim, J., Yoo, H. B., and Zhang, B.-T. Variational online mirror descent for robust learning in schrödinger bridge. *arXiv preprint arXiv:2504.02618*, 2025.

Heusel, M., Ramsauer, H., Unterthiner, T., Nessler, B., and Hochreiter, S. Gans trained by a two time-scale update rule converge to a local nash equilibrium. *Advances in neural information processing systems*, 30, 2017.

Hoffman, M. D., Gelman, A., et al. The no-u-turn sampler: adaptively setting path lengths in hamiltonian monte carlo. *J. Mach. Learn. Res.*, 15(1):1593–1623, 2014.

Karras, T., Laine, S., and Aila, T. A style-based generator architecture for generative adversarial networks. In *Proceedings of the IEEE/CVF conference on computer vision and pattern recognition*, pp. 4401–4410, 2019.

Kolesov, A., Mokrov, P., Udovichenko, I., Gazdieve, M., Pammer, G., Kratsios, A., Burnaev, E., and Korotin, A. Energy-guided continuous entropic barycenter estimation for general costs. In *Advances in Neural Information Processing Systems 37 (NeurIPS 2024)*, pp. 107513–107546. Neural Information Processing Systems Foundation, Inc., 2024.

Kornilov, N., Mokrov, P., Gasnikov, A., and Korotin, A. Optimal flow matching: Learning straight trajectories in just one step. *Advances in Neural Information Processing Systems*, 37:104180–104204, 2024.

Korotin, A., Gushchin, N., and Burnaev, E. Light schrödinger bridge. In *The Twelfth International Conference on Learning Representations*, 2024. URL <https://openreview.net/forum?id=WhZoCLRWYJ>.

Langley, P. Crafting papers on machine learning. In Langley, P. (ed.), *Proceedings of the 17th International Conference on Machine Learning (ICML 2000)*, pp. 1207–1216, Stanford, CA, 2000. Morgan Kaufmann.

Ledoux, M. and Talagrand, M. *Probability in Banach Spaces: Isoperimetry and Processes*, volume 23 of *Ergebnisse der Mathematik und ihrer Grenzgebiete (3)*. Springer, 1991.

Loshchilov, I. and Hutter, F. Decoupled weight decay regularization. *arXiv preprint arXiv:1711.05101*, 2017.

Léonard, C. A survey of the schrödinger problem and some of its connections with optimal transport, 2014. ISSN 1078-0947. URL <https://www.aimscolleges.org/article/id/d5bcf817-901d-4104-b7da-eade7847c53e>.

Mokrov, P., Korotin, A., Kolesov, A., Gushchin, N., and Bur-naev, E. Energy-guided entropic neural optimal transport. In *The Twelfth International Conference on Learning Representations*, 2024. URL <https://openreview.net/forum?id=d6tUsZeVs7>.

Peyré, G., Cuturi, M., et al. Computational optimal transport: With applications to data science. *Foundations and Trends® in Machine Learning*, 11(5-6):355–607, 2019.

Pidhorskyi, S., Adjeroh, D. A., and Doretto, G. Adversarial latent autoencoders. In *Proceedings of the IEEE/CVF Conference on Computer Vision and Pattern Recognition*, pp. 14104–14113, 2020.

Samsonov, S., Lagutin, E., Gabré, M., Durmus, A., Nau-mov, A., and Moulines, E. Local-global MCMC kernels: the best of both worlds. In Oh, A. H., Agarwal, A., Belgrave, D., and Cho, K. (eds.), *Advances in Neural Information Processing Systems*, 2022. URL <https://openreview.net/forum?id=zb-xfApk4ZK>.

Seguy, V., Damodaran, B. B., Flamary, R., Courty, N., Ro-let, A., and Blondel, M. Large scale optimal transport and mapping estimation. In *International Conference on Learning Representations*, 2018.

Shalev-Shwartz, S. and Ben-David, S. *Understanding Machine Learning: From Theory to Algorithms*. Cambridge University Press, 2014.

Shi, Y., De Bortoli, V., Campbell, A., and Doucet, A. Diffu-sion schrödinger bridge matching. *Advances in Neural Information Processing Systems*, 36:62183–62223, 2023.

Theodoropoulos, P., Komianos, N., Pacelli, V., Liu, G.-H., and Theodorou, E. A. Feedback schr\"odinger bridge matching. *arXiv preprint arXiv:2410.14055*, 2024.

Tong, A. Y., Malkin, N., Fatras, K., Atanackovic, L., Zhang, Y., Huguet, G., Wolf, G., and Bengio, Y. Simulation-free schrödinger bridges via score and flow matching. In *International Conference on Artificial Intelligence and Statistics*, pp. 1279–1287. PMLR, 2024.

Vargas, F., Thodoroff, P., Lamacraft, A., and Lawrence, N. Solving schrödinger bridges via maximum likelihood. *Entropy*, 23(9):1134, 2021.

Zhang, R., Isola, P., Efros, A. A., Shechtman, E., and Wang, O. The unreasonable effectiveness of deep features as a perceptual metric. In *Proceedings of the IEEE conference on computer vision and pattern recognition*, pp. 586–595, 2018.

Zhu, J.-Y., Park, T., Isola, P., and Efros, A. A. Unpaired image-to-image translation using cycle-consistent adver-sarial networks. In *Proceedings of the IEEE international conference on computer vision*, pp. 2223–2232, 2017.

## A. Proofs

**Notation.** Throughout the appendix, we will use the shorthand

$$Z_f := Z(f, \cdot)$$

and

$$\zeta(x_0) := \xi(x_0) + \frac{D}{2} \log(2\pi\varepsilon).$$

**Definition A.1.** Let  $\mu$  and  $\nu$  be non-negative measures on  $\mathbb{R}^d$ , and  $\mu$  absolutely continuous w.r.t.  $\nu$ . The Kullback-Leibler divergence is defined by

$$\text{KL}(\mu\|\nu) := \int \left[ \frac{d\mu}{d\nu} \log \left( \frac{d\mu}{d\nu} \right) - \frac{d\mu}{d\nu} + 1 \right] d\nu.$$

**Definition A.2** (Rademacher complexity). Let  $\mu$  be a distribution on  $X$ , and let  $\mathcal{H}$  be a class of functions  $h : X \rightarrow \mathbb{R}$ . The Rademacher complexity is defined by

$$\mathfrak{R}_N(\mathcal{H}, \mu) := \frac{1}{N} \mathbb{E} \left[ \sup_{h \in \mathcal{H}} \sum_{i=1}^N \sigma_i h(x_i) \right],$$

where  $\sigma_i \in \{-1, +1\}$  are independent Bernoulli random variables and  $x_i$  are i.i.d. samples from  $\mu$ .

The following symmetrization bound is standard; see, e.g., [Shalev-Shwartz & Ben-David \(2014, Lemma 26.2\)](#).

**Lemma A.3** (Representativeness estimation). *Let  $\mathcal{H}$  be a class of measurable functions  $h : X \rightarrow \mathbb{R}$  that are integrable with respect to  $\mu$ . Then for i.i.d. samples  $x_1, \dots, x_N \sim \mu$ ,*

$$\mathbb{E} \sup_{h \in \mathcal{H}} \left| \mathbb{E}_\mu[h] - \frac{1}{N} \sum_{i=1}^N h(x_i) \right| \leq 2 \mathfrak{R}_N(\mathcal{H}, \mu).$$

The next lemma is well known Talagran's contraction lemma [Ledoux & Talagrand \(1991, Theorem 4.12\)](#)

**Lemma A.4.** *Let  $\psi_i : \mathbb{R} \rightarrow \mathbb{R}$  be  $L$ -Lipschitz functions. Then for any collection of points  $x_i$ ,*

$$\mathbb{E}_\sigma \left[ \sup_{h \in \mathcal{H}} \sum_{i=1}^N \sigma_i \psi_i(h(x_i)) \right] \leq L \mathbb{E}_\sigma \left[ \sup_{h \in \mathcal{H}} \sum_{i=1}^N \sigma_i h(x_i) \right].$$

**Lemma A.5** (two-dimensional lemma for products of classes). *Let  $\psi : \mathbb{R}^2 \rightarrow \mathbb{R}$  be such that (23) holds on the range of values  $\{(u(x_0), v(x_0)) : u \in \mathcal{U}, v \in \mathcal{V}, x_0 \in X\}$ . Then*

$$\mathfrak{R}_N(\{\psi(u(\cdot), v(\cdot)) : u \in \mathcal{U}, v \in \mathcal{V}\}, p) \leq L_u \mathfrak{R}_N(\mathcal{U}, p) + L_v \mathfrak{R}_N(\mathcal{V}, p).$$

*Proof.* Fix a sample  $x_1, \dots, x_N$  and consider the empirical Rademacher complexity. Let  $u_i = u(x_i)$  and  $v_i = v(x_i)$ . Consider the decomposition

$$\psi(u_i, v_i) = (\psi(u_i, v_i) - \psi(0, v_i)) + \psi(0, v_i).$$

Then

$$\sup_{u \in \mathcal{U}, v \in \mathcal{V}} \sum_{i=1}^N \sigma_i \psi(u_i, v_i) \leq \sup_{u, v} \sum_{i=1}^N \sigma_i (\psi(u_i, v_i) - \psi(0, v_i)) + \sup_v \sum_{i=1}^N \sigma_i \psi(0, v_i).$$

For fixed  $v$ , the functions  $t \mapsto \psi(t, v_i) - \psi(0, v_i)$  are  $L_u$ -Lipschitz and vanish at  $t = 0$ . By Lemma A.4,

$$\mathbb{E}_\sigma \sup_u \sum_{i=1}^N \sigma_i (\psi(u_i, v_i) - \psi(0, v_i)) \leq L_u \mathbb{E}_\sigma \sup_u \sum_{i=1}^N \sigma_i u_i.$$

The right-hand side does not depend on  $v$ , so we may add  $\sup_v$  without changing it. Similarly, since  $t \mapsto \psi(0, t)$  is  $L_v$ -Lipschitz, we again apply Lemma A.4 to obtain

$$\mathbb{E}_\sigma \sup_v \sum_{i=1}^N \sigma_i \psi(0, v_i) \leq L_v \mathbb{E}_\sigma \sup_v \sum_{i=1}^N \sigma_i v_i.$$

Dividing by  $N$  and taking expectation over the sample yields the claim.  $\square$

**Lemma A.6.** *For any integrable  $f$  and  $\zeta$ , the following identity holds:*

$$\mathcal{L}(f) - \mathcal{L}(f, \zeta) = \varepsilon \mathbb{E}_{x_0 \sim p_0} \left[ \phi \left( \frac{Z_f(x_0)}{\exp \zeta(x_0)} \right) \right],$$

where  $\phi(t) := t - \log t - 1 \geq 0$ . In particular,  $\mathcal{L}(f) \geq \mathcal{L}(f, \zeta)$ , and equality holds if and only if  $\zeta(x_0) = Z_f(x_0)$  for  $p$ -a.e.  $x_0$ .

*Proof.*

$$\mathcal{L}(f) - \mathcal{L}(f, \zeta) = -\varepsilon \mathbb{E}_p[\log Z_f] + \varepsilon \mathbb{E}_p[\log \zeta] + \varepsilon \mathbb{E}_p[Z_f/\zeta] - \varepsilon = \varepsilon \mathbb{E}_p \left[ \frac{Z_f}{\zeta} - \log \frac{Z_f}{\zeta} - 1 \right].$$

□

### A.1. Proof of Proposition 3.1

*Proof.* Make the change of variables  $x_1 = x_0 + \sqrt{\varepsilon} z$ , so that  $dx_1 = \varepsilon^{D/2} dz$  and hence

$$Z(f, x_0) = (2\pi\varepsilon)^{D/2} \mathbb{E}_{z \sim \mathcal{N}(0, I)} \left[ \exp \left( \frac{f(x_0 + \sqrt{\varepsilon} z)}{\varepsilon} \right) \right] = \mathbb{E}[\exp(A(z))],$$

where

$$A(z) := \frac{f(x_0 + \sqrt{\varepsilon} z)}{\varepsilon} + \underbrace{\frac{D}{2} \log(2\pi\varepsilon)}_{\stackrel{\text{def}}{=} C}.$$

Then for any  $\xi(x_0) \in \mathbb{R}$ ,

$$\log Z = \log \mathbb{E}[e^A] = (\xi + C) + \log \mathbb{E}[e^{A-(\xi+C)}] \leq (\xi + C) + (\mathbb{E}[e^{A-(\xi+C)}] - 1),$$

using  $\log u \leq u - 1$  for all  $u > 0$ . Equality holds iff  $\mathbb{E}[e^{A-(\xi+C)}] = 1$ , i.e. when  $\xi + C = \log \mathbb{E}[e^A] = \log Z(f, x_0)$ . □

### A.2. Proof of Theorem 3.2

*Proof.* Recall the weak dual form of entropic OT (for the quadratic cost)

$$\text{EOT}_\varepsilon(p_0, p_1) = \sup_f \left\{ \mathbb{E}_{x_1 \sim p_1} [f(x_1)] - \varepsilon \mathbb{E}_{x_0 \sim p_0} [\log Z(f, x_0)] \right\},$$

where  $Z(f, x_0) = \int \exp((f(x_1) - \frac{1}{2}\|x_1 - x_0\|^2)/\varepsilon) dx_1$ . By Proposition 3.1 (with  $C = \frac{D}{2} \log(2\pi\varepsilon)$ ), for any  $\xi(x_0)$  and all  $x_0$ ,

$$\log Z(f, x_0) \leq C - 1 + \xi(x_0) + \mathbb{E}_{z \sim \mathcal{N}(0, I)} \left[ \exp \left( \frac{f(x_0 + \sqrt{\varepsilon} z)}{\varepsilon} - \xi(x_0) \right) \right].$$

Plugging this upper bound into the weak dual (and using that it holds pointwise in  $x_0$ ) yields

$$\text{EOT}_\varepsilon(p_0, p_1) \geq \sup_{f, \xi} \mathcal{L}(f, \xi).$$

Conversely, since the inequality holds for every  $\xi$ , for each fixed  $f$  we have  $\mathcal{L}(f, \xi) \leq \mathbb{E}_{p_1}[f] - \varepsilon \mathbb{E}_{p_0}[\log Z(f, x_0)]$ , hence  $\sup_{f, \xi} \mathcal{L}(f, \xi) \leq \text{EOT}_\varepsilon(p_0, p_1)$ . Finally, the bound is tight at  $\xi(x_0) + C = \log Z(f, x_0)$  (Proposition 3.1), so equality holds. Defining  $\mathcal{L}(f) := \sup_\xi \mathcal{L}(f, \xi)$  gives  $\sup_f \mathcal{L}(f) = \sup_{f, \xi} \mathcal{L}(f, \xi)$ . □

### A.3. Proof of Theorem 3.3

*Proof.* Let  $f^*$  be a maximizer of the dual problem (2), and set  $\exp \zeta^*(x_0) := Z_{f^*}(x_0)$ . Therefore,

$$\varepsilon \int \log \left( \frac{d\pi^*}{d\pi^{f, \zeta}} \right) d\pi^* = \varepsilon \int_{X_0} (\zeta(x_0) - \zeta^*(x_0)) dp(x_0) + \int_{X_1} (f^*(x_1) - f(x_1)) dp_1(x_1),$$

where we used that  $\pi^*$  has marginals  $p_0$  and  $p_1$ .

Next, we compute the total mass of  $\pi^{f,\zeta}$ :

$$\int_{X_0} \int_{X_1} p_0(x) \exp\left(\frac{f(x_1) - c(x_0, x_1)}{\varepsilon} - \zeta(x_0)\right) dx_1 dx_0 = \int_{X_0} \frac{Z_f(x_0)}{\exp \zeta(x_0)} dp(x_0).$$

Since  $\pi^*$  is a probability measure,  $\pi^*(X_0 \times X_1) = 1$ . Combining the pieces, we obtain

$$\varepsilon \text{KL}(\pi^* \parallel \pi^{f,\zeta}) = \left( \int_{X_1} f^* dp_1 - \varepsilon \int_{X_0} \zeta^* dp \right) - \left( \int_{X_1} f dp_1 - \varepsilon \int_{X_0} \zeta dp_0 - \varepsilon \int_{X_0} \frac{Z_f}{\exp \zeta} dp_0 + \varepsilon \right).$$

Finally, since  $\exp \zeta^* = Z_{f^*}$ , the first bracket equals  $\mathcal{L}(f^*) = \mathcal{L}^*$ , while the second bracket is precisely  $\mathcal{L}(f, \zeta)$  as defined in (12). Hence,

$$\varepsilon \text{KL}(\pi^* \parallel \pi^{f,\zeta}) = \mathcal{L}^* - \mathcal{L}(f, \zeta),$$

which proves (14).  $\square$

#### A.4. Proof of proposition 3.4

*Proof.* Recall  $\hat{f} = \text{argmax}_{f \in \mathcal{F}} \hat{\mathcal{L}}(f, Z(f, \cdot))$ ,  $\hat{\zeta} = \log Z_{\hat{f}}$ , then

$$\begin{aligned} \varepsilon \mathbb{E} \left[ \text{KL}(\pi^* \parallel \pi^{\hat{f}, \hat{\zeta}}) \right] &= \mathcal{L}^* - \mathcal{L}(\hat{f}, \hat{\zeta}) = \mathcal{L}^* - \sup_{f \in \mathcal{F}, \zeta \in \Xi} \mathcal{L}(f, \zeta) + \sup_{f \in \mathcal{F}, \zeta \in \Xi} \mathcal{L}(f, \zeta) - \sup_{f \in \mathcal{F}, \zeta \in \Xi} \hat{\mathcal{L}}(f, \zeta) + \\ &\underbrace{\sup_{f \in \mathcal{F}, \zeta \in \Xi} \hat{\mathcal{L}}(f, \zeta) - \hat{\mathcal{L}}(\hat{f}, \hat{\zeta}) + \hat{\mathcal{L}}(\hat{f}, \hat{\zeta}) - \mathcal{L}(\hat{f}, \hat{\zeta})}_{\leq 0} \leq 2 \sup_{f \in \mathcal{F}, \zeta \in \Xi} |\mathcal{L}(f, \zeta) - \hat{\mathcal{L}}(f, \zeta)| + \mathcal{L}^* - \sup_{f \in \mathcal{F}, \zeta \in \Xi} \mathcal{L}(f, \zeta). \end{aligned} \quad (20)$$

$\square$

#### A.5. Proof of theorem 3.5

From now on, fix classes  $\mathcal{F} \subset \text{Lip}_{L_f, M_f}(X_1)$  and  $\Xi \subset \text{Lip}_{L_\zeta, M_\zeta}(X_0)$  so:

$$\|f\|_\infty \leq M_f \quad \forall f \in \mathcal{F}, \quad 0 < \delta_\zeta := \exp(-M_\zeta) \leq \exp \zeta(x) \leq M_\zeta := \exp(M_\zeta) \quad \forall \zeta \in \Xi. \quad (21)$$

We introduce the notation  $\mathcal{E} := \{\exp(\zeta) : \zeta \in \Xi\}$  for convenience.

Our goal is to bound

$$\Delta := \sup_{f \in \mathcal{F}, \zeta \in \Xi} |\mathcal{L}(f, \zeta) - \hat{\mathcal{L}}(f, \zeta)|.$$

By the triangle inequality

$$\begin{aligned} \Delta &\leq \underbrace{\sup_{f \in \mathcal{F}} \left| \mathbb{E}_q[f] - \frac{1}{M} \sum_{j=1}^M f(y_j) \right|}_{\Delta_1} + \varepsilon \underbrace{\sup_{\zeta \in \Xi} \left| \mathbb{E}_p[\zeta] - \frac{1}{N} \sum_{i=1}^N \zeta(x_i) \right|}_{\Delta_2} + \\ &\quad + \varepsilon \underbrace{\sup_{f \in \mathcal{F}, \zeta \in \Xi} \left| \mathbb{E}_p \left[ \frac{Z_f}{\zeta} \right] - \frac{1}{N} \sum_{i=1}^N \left[ \frac{Z_f}{\exp \zeta} \right](x_i) \right|}_{\Delta_3}. \end{aligned} \quad (22)$$

By Lemma A.3,

$$\mathbb{E}[\Delta_1] \leq 2 \mathfrak{R}_M(\mathcal{F}, q),$$

$$\mathbb{E}[\Delta_2] \leq 2 \mathfrak{R}_N(\Xi, p),$$

where all bounds are taken in expectation with respect to the random samples.

Consider the classes

$$\mathcal{Z} := \{Z(f, \cdot) : f \in \mathcal{F}\}, \quad \mathcal{H}_{\text{frac}} := \left\{ \frac{Z(f, \cdot)}{\exp \zeta} : f \in \mathcal{F}, \zeta \in \Xi \right\}.$$

We first obtain a crude upper bound on  $Z(f, \cdot)$ . From (21) it follows that

$$0 < Z(f, x_0) \leq e^{M_f/\varepsilon} \int_{\mathbb{R}^D} \exp \left( \frac{-\|x_0 - x_1\|^2}{2\varepsilon} \right) dx_1 = (2\pi\varepsilon)^{D/2} \cdot e^{M_f/\varepsilon} =: M_Z.$$

Define  $\psi(u, v) = u/v$  on the rectangle  $u \in [0, M_Z]$ ,  $v \in [\delta_{\mathcal{E}}, M_{\mathcal{E}}]$ . Then

$$\left| \frac{\partial \psi}{\partial u} \right| = \frac{1}{v} \leq \frac{1}{\delta_{\mathcal{E}}} =: L_u, \quad \left| \frac{\partial \psi}{\partial v} \right| = \frac{u}{v^2} \leq \frac{M_Z}{\delta_{\mathcal{E}}^2} =: L_v.$$

Therefore, for any  $u, u' \in [0, M_Z]$  and  $v, v' \in [\delta_{\mathcal{E}}, M_{\mathcal{E}}]$ ,

$$|\psi(u, v) - \psi(u', v')| \leq L_u |u - u'| + L_v |v - v'|. \quad (23)$$

Applying Lemma A.3 to the class  $\mathcal{H}_{\text{frac}}$  and then Lemma A.5 to  $\psi(u, v) = u/v$ , with  $\mathcal{U} = \mathcal{Z}$  and  $\mathcal{V} = \mathcal{E}$ , we obtain

$$\mathbb{E}[\Delta_3] \leq 2 \mathfrak{R}_N(\mathcal{H}_{\text{frac}}, p) \leq 2 \left( \frac{1}{\delta_{\mathcal{E}}} \mathfrak{R}_N(\mathcal{Z}, p) + \frac{M_Z}{\delta_{\mathcal{E}}^2} \mathfrak{R}_N(\mathcal{E}, p) \right) \leq 2 \left( \frac{1}{\delta_{\mathcal{E}}} \mathfrak{R}_N(\mathcal{Z}, p) + \frac{M_Z M_{\mathcal{E}}}{\delta_{\mathcal{E}}^2} \mathfrak{R}_N(\Xi, p) \right).$$

where in last inequality we use Lemma A.4 for class  $\Xi$  and function  $\exp(\cdot)$  on  $[-M_{\zeta}, M_{\zeta}]$ .

Collecting the bounds, we get

$$\mathbb{E}[\Delta] \leq 2 \mathfrak{R}_M(\mathcal{F}, q) + \frac{2\varepsilon}{\delta_{\mathcal{E}}} \mathfrak{R}_N(\Xi, p) + 2\varepsilon \left( \frac{1}{\delta_{\mathcal{E}}} \mathfrak{R}_N(\mathcal{Z}, p) + \frac{M_Z M_{\mathcal{E}}}{\delta_{\mathcal{E}}^2} \mathfrak{R}_N(\Xi, p) \right). \quad (24)$$

It remains to characterize the asymptotic behavior of each Rademacher complexity term appearing in the inequality above as a function of the corresponding sample sizes. Bounds for  $\mathfrak{R}(\mathcal{F}, p_1)$  and  $\mathfrak{R}(\Xi, p_0)$  follow directly from Gottlieb et al. (2016, Theorem 4.3), namely,

$$\mathfrak{R}(\mathcal{F}, p_1) \leq O\left(M^{-\frac{1}{1+D}}\right), \quad \mathfrak{R}(\Xi, p_0) \leq O\left(N^{-\frac{1}{1+D}}\right).$$

Finally, the Rademacher complexity of the induced class  $\mathfrak{R}(\mathcal{Z}, p_0)$  is controlled in Kolesov et al. (2024, Theorem 4.5) and satisfies the same rate,

$$\mathfrak{R}(\mathcal{Z}, p_0) \leq O\left(N^{-\frac{1}{2}}\right) \leq O\left(N^{-\frac{1}{1+D}}\right).$$

## A.6. Proof of theorem 3.7

*Proof.* Let  $X_0 := \text{supp}(p_0) \subset \mathbb{R}^D$  and  $X_1 := \text{supp}(p_1) \subset \mathbb{R}^D$  be compact, and  $c(x_0, x_1) = \frac{1}{2}\|x_0 - x_1\|^2$ . Fix  $\delta > 0$ . We use that  $\mathcal{L}$  is invariant under additive shifts: for any  $t \in \mathbb{R}$ ,

$$\mathcal{L}(f + t) = \int_{\mathbb{R}^D} (f + t) dp_1 - \varepsilon \int_{\mathbb{R}^D} \log \int_{\mathbb{R}^D} e^{(f(x_1) + t - c(x_0, x_1))/\varepsilon} dx_1 dp_0(x_0) = \mathcal{L}(f).$$

Assume  $\mathcal{L}^* < \infty$  and let  $f^* : \mathbb{R}^D \rightarrow [-\infty, \infty)$  be an extended-real optimizer such that  $f^*(x_1) > -\infty$  for  $x_1 \in X_1$  and  $f^*(x_1) = -\infty$  for  $x_1 \notin X_1$  (hence  $Z_{f^*}(x_0) = \int_{X_1} e^{(f^*(x_1) - c(x_0, x_1))/\varepsilon} dx_1$ ). By shift-invariance we normalize  $\sup_{x_1 \in X_1} f^*(x_1) = 0$ .

Since  $X_1$  is compact and  $\varepsilon > 0$ , the maximizer can be chosen with continuous restriction to  $X_1$ ; therefore we may pick a Lipschitz function  $g : X_1 \rightarrow \mathbb{R}$  with Lipschitz constant  $L_g$  such that

$$\|g - f^*\|_{\infty, X_1} \leq \eta, \quad \text{and} \quad \sup_{X_1} g = 0,$$

where  $\eta > 0$  will be chosen below. Set  $B := \|g\|_{\infty, X_1}$  and choose  $M > B$ .

For any  $L \geq L_g$ , define the  $L$ -Lipschitz extension

$$\tilde{g}_L(x_1) := \sup_{z \in X_1} (g(z) - L\|x_1 - z\|), \quad x_1 \in \mathbb{R}^D,$$

so that  $\tilde{g}_L|_{X_1} = g$  and  $\tilde{g}_L$  is  $L$ -Lipschitz on  $\mathbb{R}^D$ . Define the bounded Lipschitz potential

$$f_{L,M}(x_1) := \max\{-M, \tilde{g}_L(x_1)\}, \quad x_1 \in \mathbb{R}^D,$$

which is  $L$ -Lipschitz and satisfies  $-M \leq f_{L,M} \leq 0$ . Moreover, writing  $t := (M + B)/L$  and

$$X_1^t := \{x_1 \in \mathbb{R}^D : \text{dist}(x_1, X_1) \leq t\},$$

we have  $f_{L,M}(x_1) = -M$  for all  $x_1 \notin X_1^t$  because  $\tilde{g}_L(x_1) \leq B - L \text{dist}(x_1, X_1)$ .

We bound  $\mathcal{L}(f^*) - \mathcal{L}(f_{L,M})$ . Since  $p_1$  is supported on  $X_1$  and  $f_{L,M}|_{X_1} = g$ ,

$$\int_{\mathbb{R}^D} f_{L,M} \, dp_1 = \int_{X_1} g \, dp_1, \quad \left| \int_{X_1} g \, dp_1 - \int_{X_1} f^* \, dp_1 \right| \leq \eta.$$

For the partition functions, for any  $x_0 \in X_0$  we write

$$Z_{f_{L,M}}(x_0) = \int_{X_1} e^{(g(x_1) - c(x_0, x_1))/\varepsilon} \, dx_1 + \int_{X_1^t \setminus X_1} e^{(f_{L,M}(x_1) - c(x_0, x_1))/\varepsilon} \, dx_1 + \int_{(X_1^t)^c} e^{(-M - c(x_0, x_1))/\varepsilon} \, dx_1.$$

On  $X_1$ , the uniform approximation implies

$$e^{-\eta/\varepsilon} Z_{f^*}(x_0) \leq \int_{X_1} e^{(g - c(x_0, \cdot))/\varepsilon} \, dx_1 \leq e^{\eta/\varepsilon} Z_{f^*}(x_0).$$

Let  $\lambda$  denote Lebesgue measure and define

$$C_\varepsilon := \int_{\mathbb{R}^D} e^{-\|u\|^2/\varepsilon} \, du = (\pi\varepsilon)^{D/2}.$$

Using  $f_{L,M} \leq 0$  and  $c \geq 0$  on  $X_1^t \setminus X_1$ , and  $f_{L,M} = -M$  on  $(X_1^t)^c$ , we have for all  $x_0 \in X_0$ ,

$$\int_{X_1^t \setminus X_1} e^{(f_{L,M} - c(x_0, \cdot))/\varepsilon} \, dx_1 \leq \lambda(X_1^t \setminus X_1), \quad \int_{(X_1^t)^c} e^{(-M - c(x_0, x_1))/\varepsilon} \, dx_1 \leq e^{-M/\varepsilon} \int_{\mathbb{R}^D} e^{-\|x_0 - x_1\|^2/\varepsilon} \, dx_1 = e^{-M/\varepsilon} C_\varepsilon.$$

To control the logarithm we need a uniform positive lower bound. Since  $g$  is continuous on compact  $X_1$ , let  $m := \inf_{X_1} g > -\infty$  and  $C_{X_0, X_1} := \sup_{(x_0, x_1) \in X_0 \times X_1} \|x_0 - x_1\|^2 < \infty$ . If  $\lambda(X_1) = 0$ , then  $Z_{f^*}(x_0) = \int_{X_1} e^{(f^* - c(x_0, \cdot))/\varepsilon} \, dx_1 = 0$  and  $\mathcal{L}(f^*) = +\infty$ , contradicting  $\mathcal{L}^* < \infty$ ; hence  $\lambda(X_1) > 0$  and

$$\int_{X_1} e^{(g - c(x_0, \cdot))/\varepsilon} \, dx_1 \geq \lambda(X_1) \exp\left(\frac{m - C_{X_0, X_1}}{\varepsilon}\right) =: \underline{Z} > 0.$$

Combining, and using  $Z_{f^*}(x_0) \geq e^{-\eta/\varepsilon} \int_{X_1} e^{(g - c(x_0, \cdot))/\varepsilon} \, dx_1 \geq e^{-\eta/\varepsilon} \underline{Z}$ , we obtain for all  $x_0 \in X_0$ ,

$$Z_{f_{L,M}}(x_0) \leq e^{\eta/\varepsilon} Z_{f^*}(x_0) + \lambda(X_1^t \setminus X_1) + e^{-M/\varepsilon} C_\varepsilon \leq e^{\eta/\varepsilon} Z_{f^*}(x_0) \left(1 + \frac{\lambda(X_1^t \setminus X_1) + e^{-M/\varepsilon} C_\varepsilon}{e^{-\eta/\varepsilon} \underline{Z}}\right),$$

hence, by  $\log(1 + u) \leq u$  for  $u \geq 0$ ,

$$\log Z_{f_{L,M}}(x_0) - \log Z_{f^*}(x_0) \leq \eta/\varepsilon + \frac{\lambda(X_1^t \setminus X_1) + e^{-M/\varepsilon} C_\varepsilon}{e^{-\eta/\varepsilon} \underline{Z}}.$$

Therefore

$$\mathcal{L}(f^*) - \mathcal{L}(f_{L,M}) \leq \eta + \varepsilon \int_{X_0} (\log Z_{f_{L,M}} - \log Z_{f^*}) \, dp \leq 2\eta + \varepsilon \frac{\lambda(X_1^t \setminus X_1) + e^{-M/\varepsilon} C_\varepsilon}{e^{-\eta/\varepsilon} \underline{Z}}.$$

Since  $X_1$  is compact,  $\lambda(X_1^t) < \infty$  for all  $t > 0$  and  $X_1^t \downarrow X_1$  as  $t \downarrow 0$ , so by continuity from above  $\lambda(X_1^t \setminus X_1) = \lambda(X_1^t) - \lambda(X_1) \rightarrow 0$  as  $t \rightarrow 0$ . Choose first  $\eta > 0$  so that  $2\eta \leq \delta/4$ , then choose  $M$  so that  $\varepsilon e^{-M/\varepsilon} C_\varepsilon / (e^{-\eta/\varepsilon} \underline{Z}) \leq \delta/8$ , and then choose  $L$  large enough so that with  $t = (M + B)/L$  one has  $\varepsilon \lambda(X_1^t \setminus X_1) / (e^{-\eta/\varepsilon} \underline{Z}) \leq \delta/8$ . This yields

$$\mathcal{L}(f_{L,M}) \geq \mathcal{L}(f^*) - \delta/2 = \mathcal{L}^* - \delta/2.$$

Now let  $\{\mathcal{F}_n\}_{n \geq 1}$  be an increasing sequence of function classes such that for some sequences  $L_n \uparrow \infty$ ,  $M_n \uparrow \infty$  one has

$$\{f : \mathbb{R}^D \rightarrow \mathbb{R} \text{ } L_n\text{-Lipschitz and } \|f\|_\infty \leq M_n\} \subseteq \mathcal{F}_n.$$

Pick  $n$  such that  $L_n \geq L$  and  $M_n \geq M$ ; then  $f_{L,M} \in \mathcal{F}_n$ , and hence

$$\sup_{f \in \mathcal{F}_n} \mathcal{L}(f) \geq \mathcal{L}(f_{L,M}) \geq \mathcal{L}^* - \delta/2,$$

which implies  $\mathcal{L}^* - \sup_{f \in \mathcal{F}_n} \mathcal{L}(f) < \delta$ .

It remains to note that the one-potential objective can be written in the two-potential form:

$$\mathcal{L}(f) = \mathcal{L}(f, \zeta_f), \quad \zeta_f(x_0) := -\varepsilon \log Z_f(x_0),$$

so that maximizing  $\mathcal{L}(f)$  over  $f$  is equivalent, to maximizing  $\mathcal{L}(f, \zeta)$  over pairs  $(f, \zeta)$  with  $\zeta = \zeta_f$ . Moreover, for bounded  $f$  the function  $\log Z_f$  is bounded and Lipschitz on  $\mathbb{R}^D$  (hence  $\zeta_f$  is bounded and Lipschitz as well). Therefore, choosing  $L_\zeta$  and  $M_\zeta$  sufficiently large and taking  $n$  large enough, we ensure that  $\zeta_f \in \Xi_n$  for every  $f \in \mathcal{F}_n$ , and consequently

$$\sup_{f \in \mathcal{F}_n, \zeta \in \Xi_n} \mathcal{L}(f, \zeta) \geq \sup_{f \in \mathcal{F}_n} \mathcal{L}(f, \zeta_f) = \sup_{f \in \mathcal{F}_n} \mathcal{L}(f).$$

Combining this with the previously established bound  $\mathcal{L}^* - \sup_{f \in \mathcal{F}_n} \mathcal{L}(f) < \delta$  yields the desired approximation statement for  $\sup_{f \in \mathcal{F}_n, \zeta \in \Xi_n} \mathcal{L}(f, \zeta)$ .  $\square$

## B. Details of the Experiments

### B.1. VarEOT: Optimization and Architecture

**Optimization.** Training is performed using the AdamW (Loshchilov & Hutter, 2017) optimizer with a learning rate  $\text{lr} = 10^{-4}$ , momentum parameters  $\beta_1 = 0.7$  and  $\beta_2 = 0.8$ , and weight decay set to  $10^{-4}$ . We additionally employ an exponential moving average (EMA) of model parameters with momentum  $\text{ema\_momentum} = 0.999$ , which is used for evaluation. All models are trained for  $10^4$  gradient steps.

**Network architecture.** The transport potential is parameterized by a multilayer perceptron (MLP). The network consists of four fully connected layers with SiLU activations. The input dimensionality is denoted by  $d_{\text{in}}$  (512 for latent-space experiments), the hidden layer width is fixed to 256 units, and the output dimension is  $d_{\text{out}} = 1$ .

**Training setup.** All models are trained with a batch size of 256. The number of Monte Carlo samples used to estimate expectations is fixed to  $K = 256$  across all experiments.

**Langevin inference.** The number of Langevin steps  $S$  (denoted as NFE) and the corresponding step size are chosen depending on the experimental setting. For all toy experiments on the SwissRoll dataset, we use 1000 Langevin steps with a fixed step size of  $10^{-3}$ . For image-based experiments in the ALAE latent space, we consider multiple inference budgets. The step sizes for each NFE configuration are selected based on FID performance, as illustrated in Figure 7. Specifically, we use a step size of 0.5 for NFE = 2, a step size of 0.1 for NFE = 10, and a step size of  $10^{-3}$  for NFE = 1000.

**Update schedule and practical considerations.** While the algorithmic description in 1 includes an iterative optimization scheme in which the potential network parameters  $\theta$  are updated every  $\Theta_{\text{step}}$  iterations, we found that, in practice, a simpler update schedule leads to more stable training and better empirical performance.

Specifically, we perform simultaneous optimization of both the dual potential network  $\hat{f}_\theta$  and the auxiliary network  $\hat{\xi}_\psi$  at every training step.

## B.2. Baseline Methods

For completeness, we summarize the main technical details of the baseline methods used for comparison in the unpaired image-to-image translation experiments.

**LightSB.** For LightSB, we follow the standard configuration reported in prior work. The model is trained using  $K = 10$  Gaussian components, a learning rate of  $\text{lr} = 10^{-3}$ , and a batch size of 128. Optimization is performed for  $10^4$  gradient steps.

**EgNOT.** For EgNOT, we follow the optimization/hyperparameter setup from the original work, but adopt the same neural network architecture for potential  $f$  as in section B.1 for fair comparison with VarEOT. Training/inference hyperparameters were selected by grid search over a reasonable parameter space based on FID performance. For all ALAE experiments, Adam optimizer is used with  $\text{lr} = 5 \cdot 10^{-5}$ ,  $(\beta_1, \beta_2) = (0, 0.999)$ . Optimization is performed for  $10^4$  gradient steps, batch size is 128.

## B.3. Image Data and Preprocessing

For image-based experiments, we rely on the official implementation of ALAE and the corresponding pretrained models, available at

<https://github.com/podgorskiy/ALAE>

To obtain semantic attributes for the FFHQ dataset, we use the neural network-based annotations released at

<https://github.com/DCGM/ffhq-features-dataset>

For baseline comparisons, we use the official implementations of LightSB and EgNOT, available at

<https://github.com/ngushchin/LightSB>

and

<https://github.com/PetrMokrov/Energy-guided-Entropic-OT>

respectively.

## C. Additional Experimental Results

### C.1. Other Unpaid Image-to-Image Translation setups

In the main text, we present qualitative results for the unpaired image-to-image translation task using the ALAE encoder in the Male-to-Female ( $M \rightarrow F$ ) setup. In this appendix, we provide additional qualitative examples for the same task under alternative and commonly used translation directions.

Specifically, we report results for the Woman-to-Man ( $F \rightarrow M$ ), Adult-to-Child ( $A \rightarrow C$ ), and Child-to-Adult ( $C \rightarrow A$ ) setups. All experiments are conducted under the same training protocol and model configuration as in the main text, and differ only in the choice of the source and target domains. For consistency, we fix the regularization parameter to  $\varepsilon = 1.0$  for all setups shown below.

Figures 3–5 demonstrate that the proposed method successfully learns meaningful transport maps across different translation directions, further confirming that the qualitative behavior observed in the  $M \rightarrow F$  setup generalizes to other unpaired image-to-image translation scenarios.

### C.2. Dependence on the parameter $\varepsilon$ .

In Figure 6, we show how the solution learned by VarEOT depends on the parameter  $\varepsilon$  in the *Male*→*Female* experiment. As expected, the diversity increases with the increase of  $\varepsilon$ .

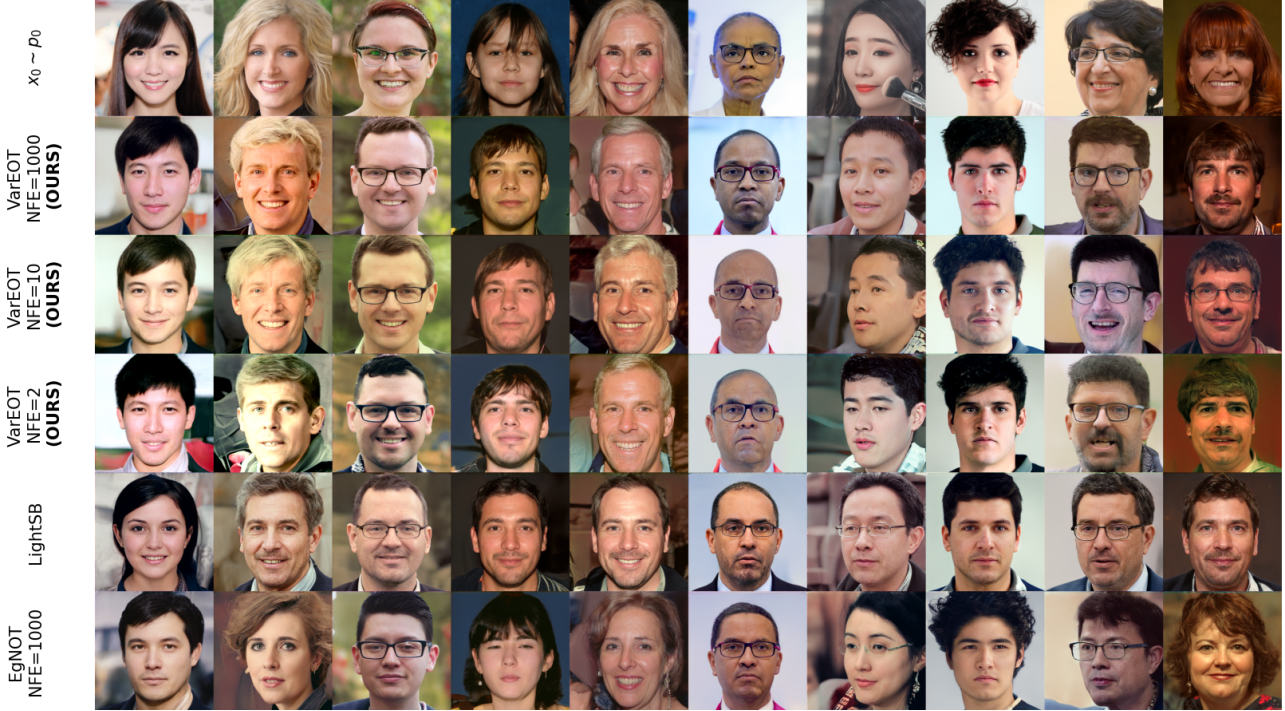


Figure 3. Qualitative comparison for *Female* → *Male* translation with  $\varepsilon = 1.0$ . From top to bottom: input samples, VarEOT (ours), LightSB, and EgNOT. Input images are selected from the test set: we take the first 300 samples and rank them by encoder-decoder reconstruction quality (LPIPS), displaying the top-ranked examples.

### C.3. Effect of Langevin Inference Parameters

To further analyze the behavior of VarEOT at inference time, we study the sensitivity of the translation quality to the Langevin sampling parameters in the *Male* → *Female* (M → F) image-to-image translation task. Figure 7 reports heatmaps of FID scores as a function of the Langevin step size and the number of sampling steps, for different values of the entropic regularization parameter  $\varepsilon$ .



Figure 4. Qualitative comparison for *Adult*  $\rightarrow$  *Child* translation with  $\varepsilon = 1.0$ . From top to bottom: input samples, VarEOT (ours), LightSB, and EgNOT. Input images are selected from the test set: we take the first 300 samples and rank them by encoder-decoder reconstruction quality (LPIPS), displaying the top-ranked examples.



Figure 5. Qualitative comparison for *Child*  $\rightarrow$  *Adult* translation with  $\varepsilon = 1.0$ . From top to bottom: input samples, VarEOT (ours), LightSB, and EgNOT. Input images are selected from the test set: we take the first 300 samples and rank them by encoder-decoder reconstruction quality (LPIPS), displaying the top-ranked examples.



(a) VarEOT  $Male \rightarrow Female$ ,  $\varepsilon = 0.1$ . Almost no diversity.



(b) VarEOT  $Male \rightarrow Female$ ,  $\varepsilon = 0.5$ . Resonable diversity.



(c) VarEOT  $Male \rightarrow Female$ ,  $\varepsilon = 1.0$ . Moderate diversity.



(d) VarEOT  $Male \rightarrow Female$ ,  $\varepsilon = 10.0$ . High diversity.

Figure 6. VarEOT with NFE=10 in task:  $Man \rightarrow Woman$  for different  $\varepsilon$

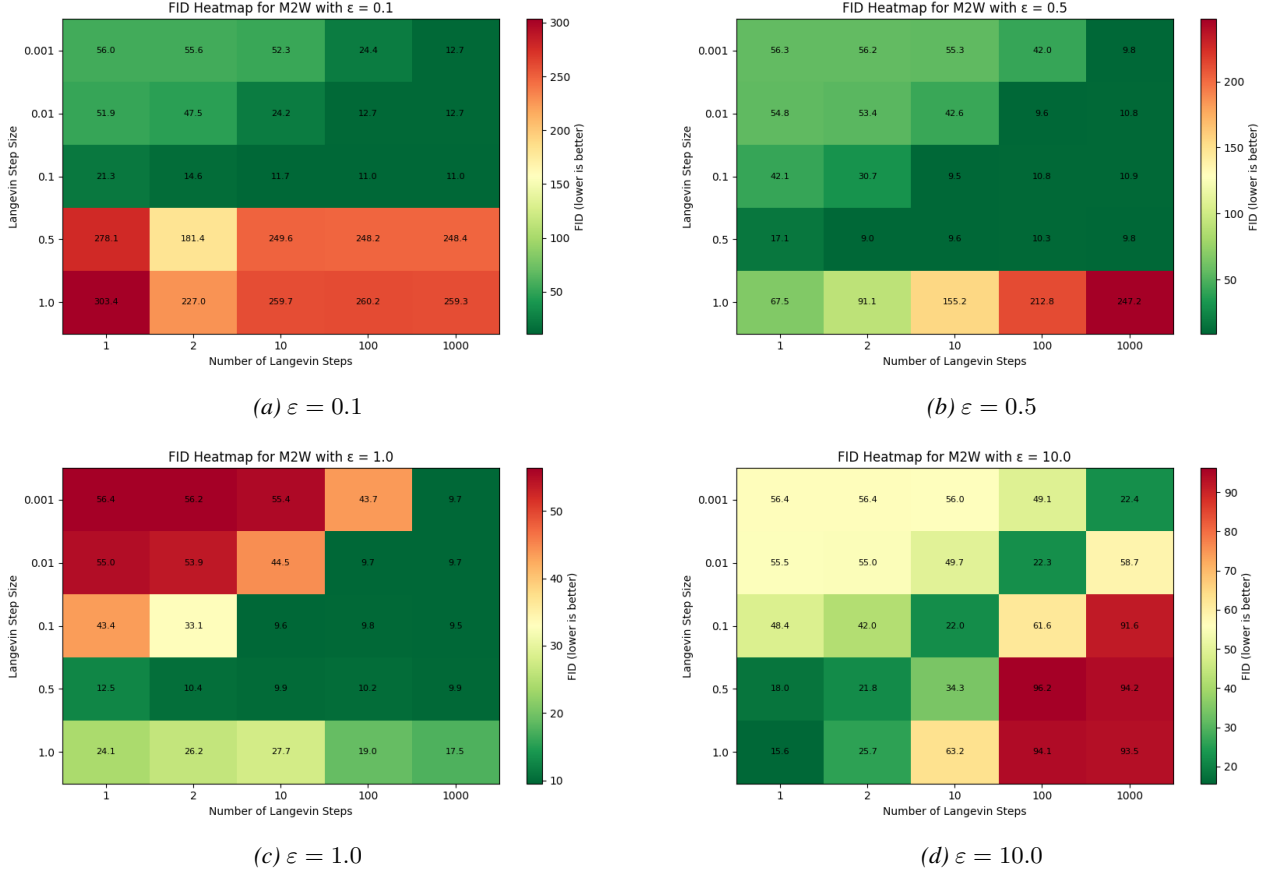


*Figure 7.* FID heatmaps for the *Male*→*Female* (M→F) unpaired image-to-image translation task in the ALAE latent space. Each heatmap shows the dependence of FID on the Langevin step size (rows) and the number of inference steps (columns) for a fixed value of the entropic regularization parameter  $\varepsilon$ . Lower values indicate better performance.